Supplementary information for

Exploration of new second-order nonlinear optical materials in the Cs-Hg-Br-I systems

Qi Wu [a], Yin Huang [a], Xianggao Meng [b], Cheng Zhong [a], Xingguo Chen [a] and Jingui Qin [a]**

[a]Department of Chemistry, Wuhan University, Wuhan 430072, China

[b]College of Chemistry, Central China Normal University, Wuhan 430079, China

Captions of the figures

Figure S1. X-ray diffraction powder patterns for $Cs_2Hg_2Br_2I_4 \cdot H_2O$: Calculated and experimental

Figure S2. X-ray diffraction powder patterns for $Cs_2Hg_3I_8 \cdot H_2O$: Calculated and experimental.

Figure S3. Phase-matching curve for $Cs_2Hg_2Br_2I_4 \cdot H_2O$.

Figure S4. Phase-matching curve for $Cs_2Hg_3I_8 \cdot H_2O$.

Figure S5. ATR-FTIR spectrum for $Cs_2Hg_2Br_2I_4 \cdot H_2O$.

Figure S6. Raman spectrum for $Cs_2Hg_2Br_2I_4 \cdot H_2O$.

Figure S7. ATR-FTIR spectrum for $Cs_2Hg_3I_8 \cdot H_2O$.

Figure S8. Raman spectrum for $Cs_2Hg_3I_8 \cdot H_2O$.

Figure S9. UV-Vis absorption spectrum for $Cs_2Hg_2Br_2I_4 \cdot H_2O$.

Figure S10. UV-Vis absorption spectrum for $Cs_2Hg_3I_8 \cdot H_2O$.

Figure S11. Total and partial density of states for compounds $Cs_2Hg_2Br_2I_4 \cdot H_2O$ using the rPBE/norm-conserving pseudopotential method.

Figure S12. Total and partial density of states for compounds $Cs_2Hg_3I_8 \cdot H_2O$ using the rPBE/norm-conserving pseudopotential method.

Figure S13. The band structure of $Cs_2Hg_2Br_2I_4 \cdot H_2O$.

Figure S14. The band structure of $Cs_2Hg_3I_8 \cdot H_2O$.

Figure S15. Calculated Refractive Indices for $Cs_2Hg_2Br_2I_4 \cdot H_2O$.

Figure S16. Calculated Refractive Indices for $Cs_2Hg_2Br_2I_4 \cdot H_2O$.

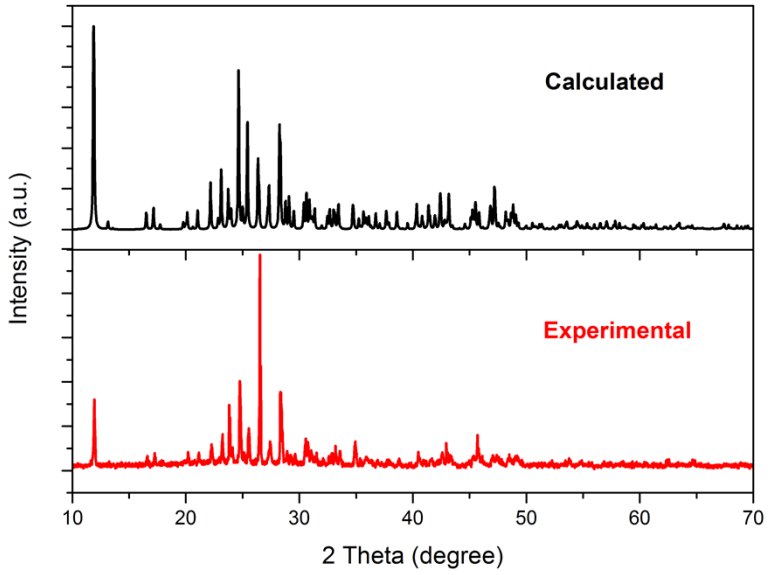

Figure S1. X-ray diffraction powder patterns for $Cs_2Hg_2Br_2I_4 \cdot H_2O$: Calculated and experimental.

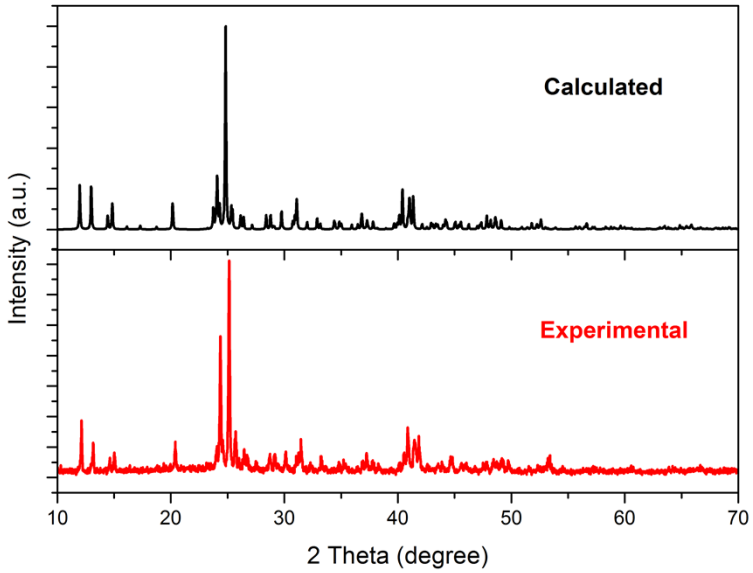

Figure S2. X-ray diffraction powder patterns for $Cs_2Hg_3I_8 \cdot H_2O$: Calculated and experimental

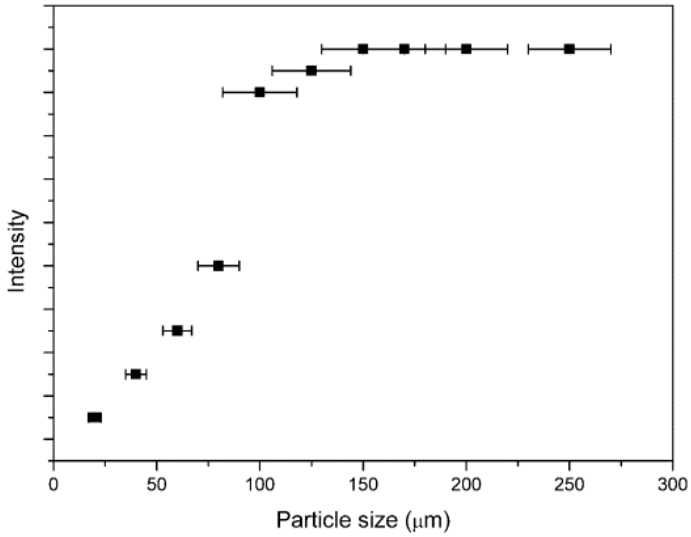

Figure S3. Phase-matching curve for $Cs_2Hg_2Br_2I_4 \cdot H_2O$.

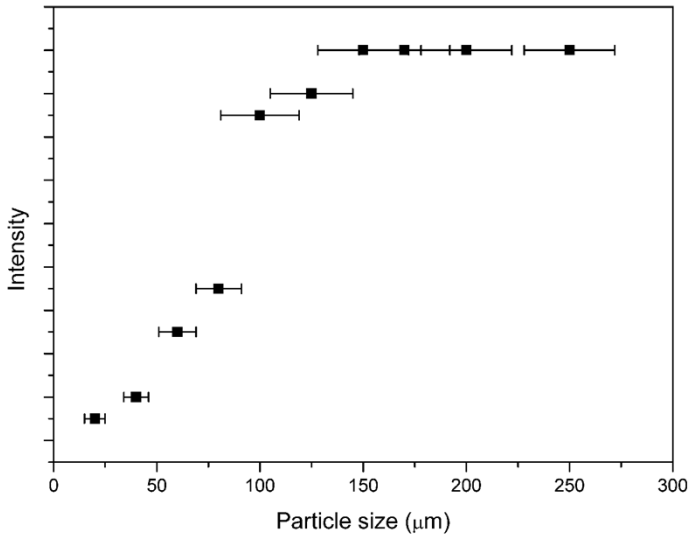

Figure S4. Phase-matching curve for $Cs_2Hg_3I_8 \cdot H_2O$.

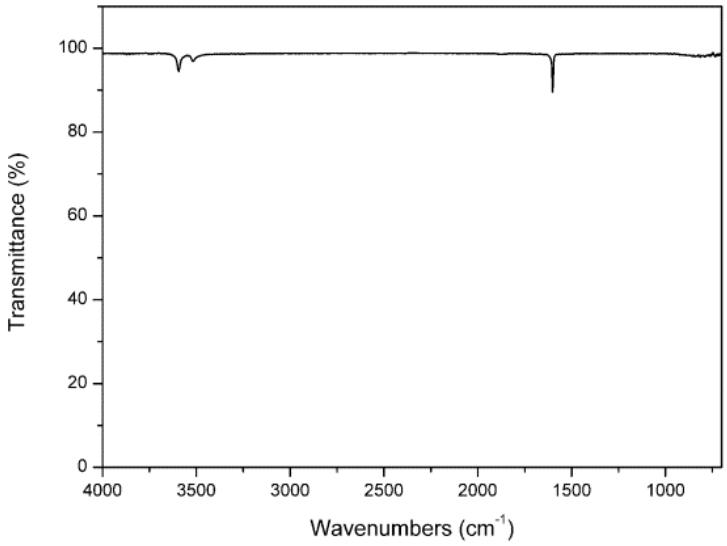

Figure S5. ATR-FTIR spectrum for $Cs_2Hg_2Br_2I_4 \cdot H_2O$.

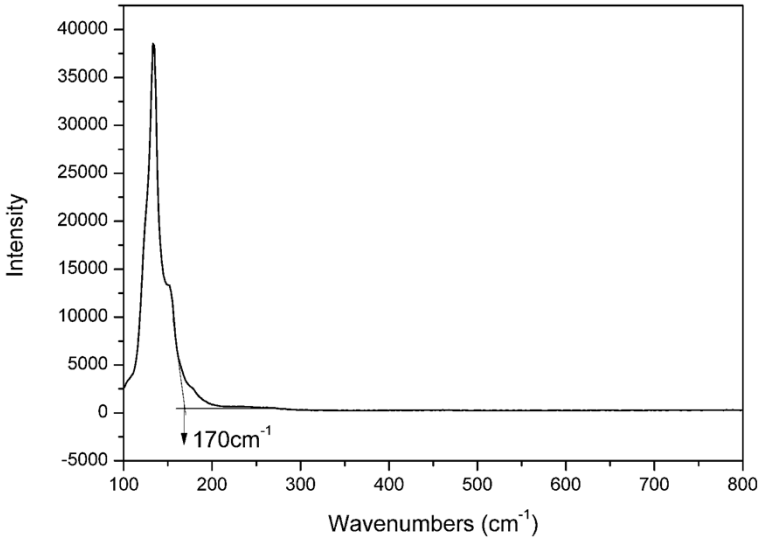

Figure S6. Raman spectrum for $Cs_2Hg_2Br_2I_4 \cdot H_2O$.

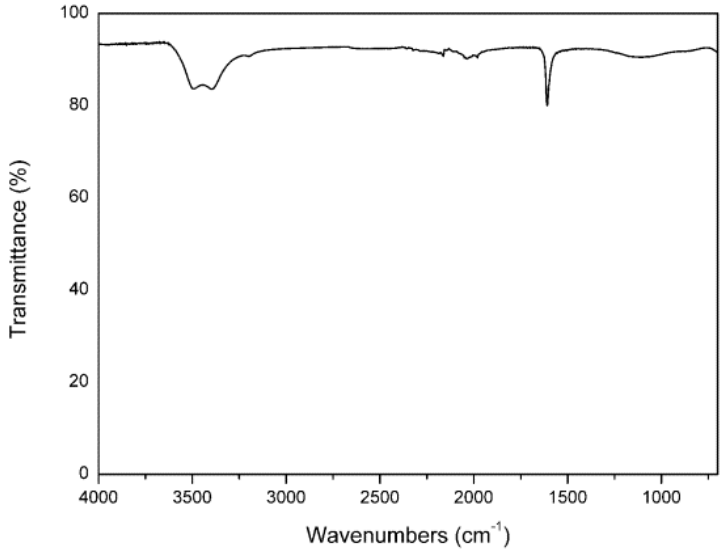

Figure S7. ATR-FTIR spectrum for $Cs_2Hg_3I_8 \cdot H_2O$.

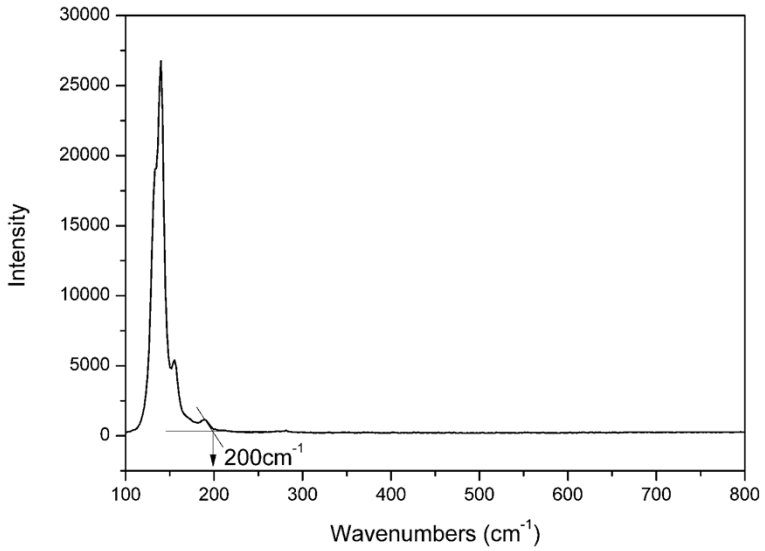

Figure S8. Raman spectrum for $Cs_2Hg_3I_8 \cdot H_2O$.

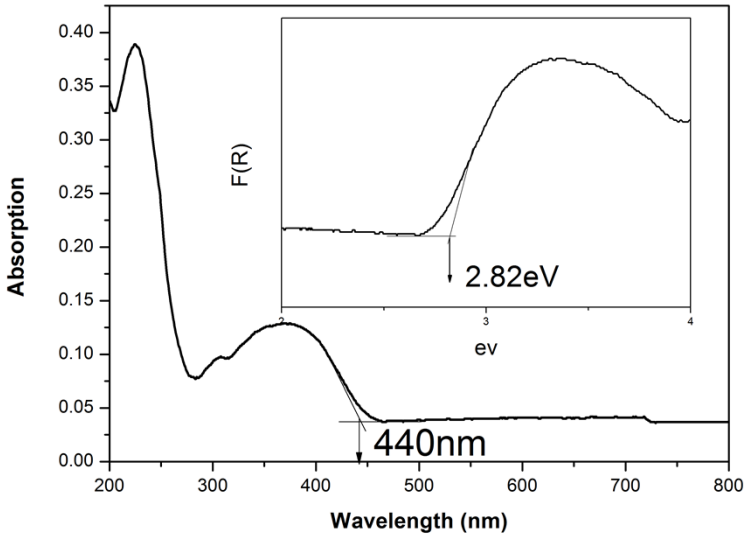

Figure S9. UV-Vis absorption spectrum for $Cs_2Hg_2Br_2I_4 \cdot H_2O$.

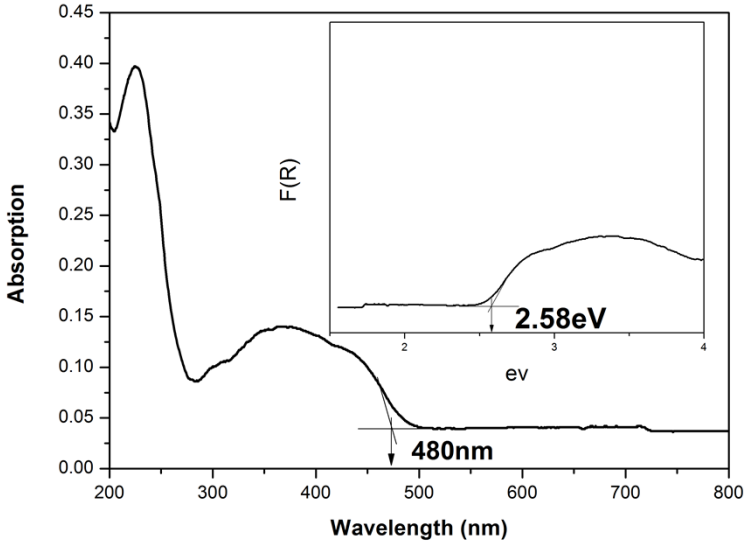

Figure S10. UV-Vis absorption spectrum for $Cs_2Hg_3I_8 \cdot H_2O$.

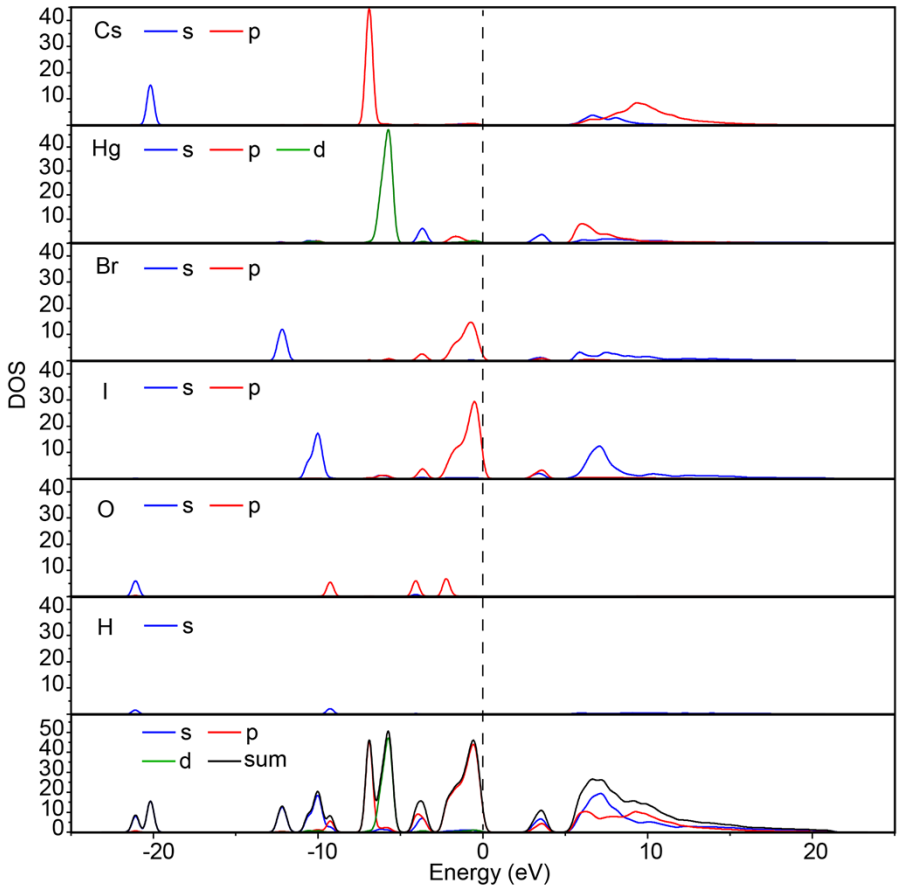

Figure S11. Total and partial density of states for compounds $Cs_2Hg_2Br_2I_4 \cdot H_2O$ using the rPBE/norm-conserving pseudopotential method.

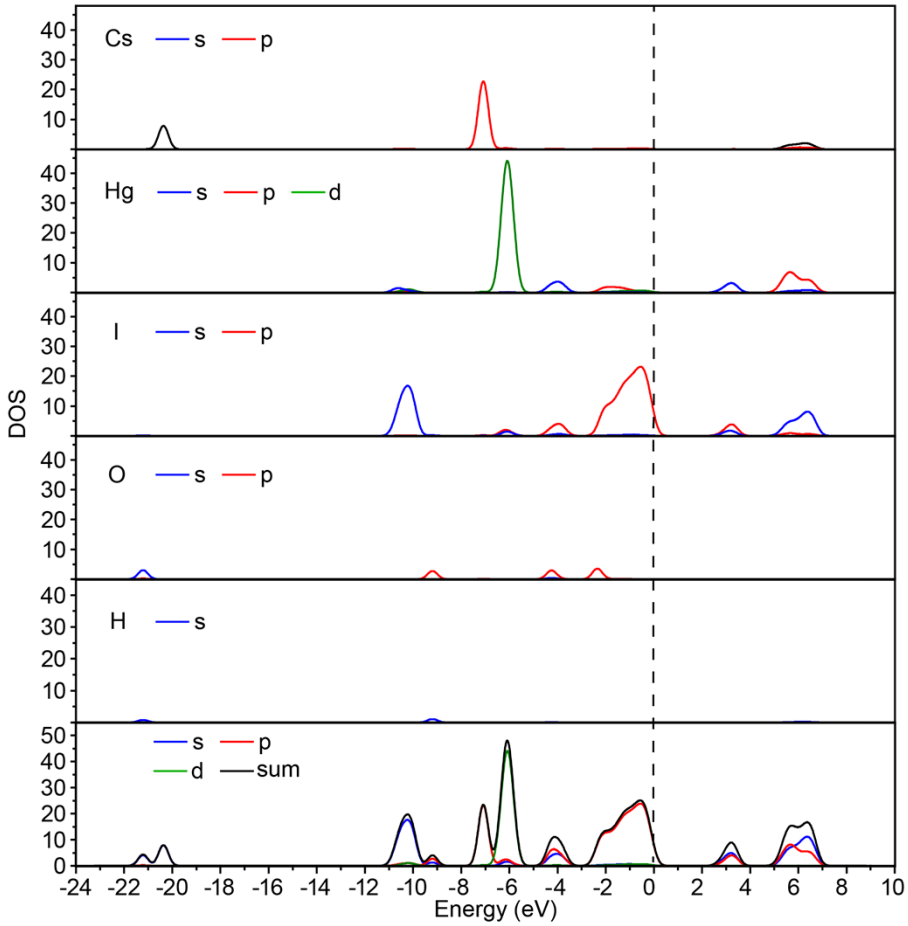

Figure S12. Total and partial density of states for compounds $Cs_2Hg_3I_8 \cdot H_2O$ using the rPBE/norm-conserving pseudopotential method.

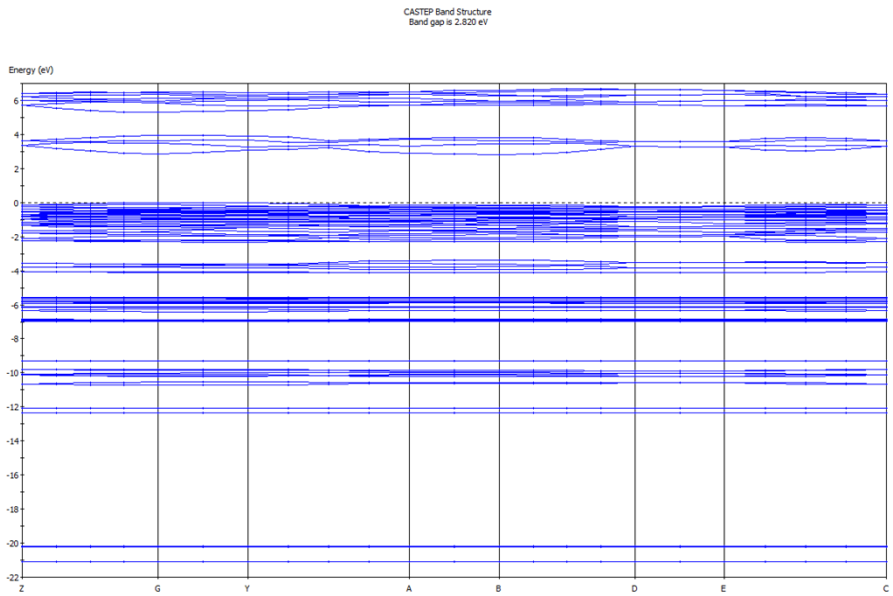

Figure S13. The band structures of $Cs_2Hg_2Br_2I_4 \cdot H_2O$.

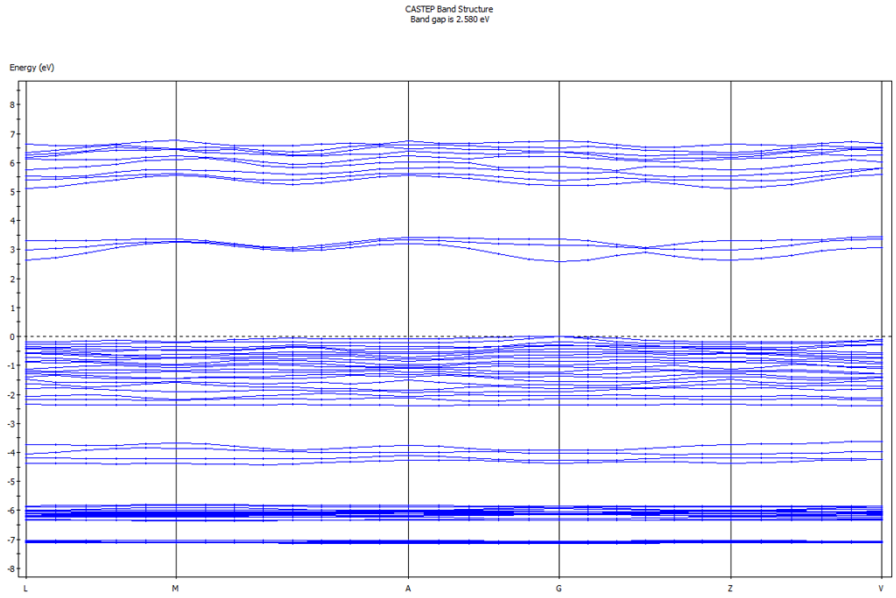

Figure S14. The band structures of $Cs_2Hg_3I_8 \cdot H_2O$.

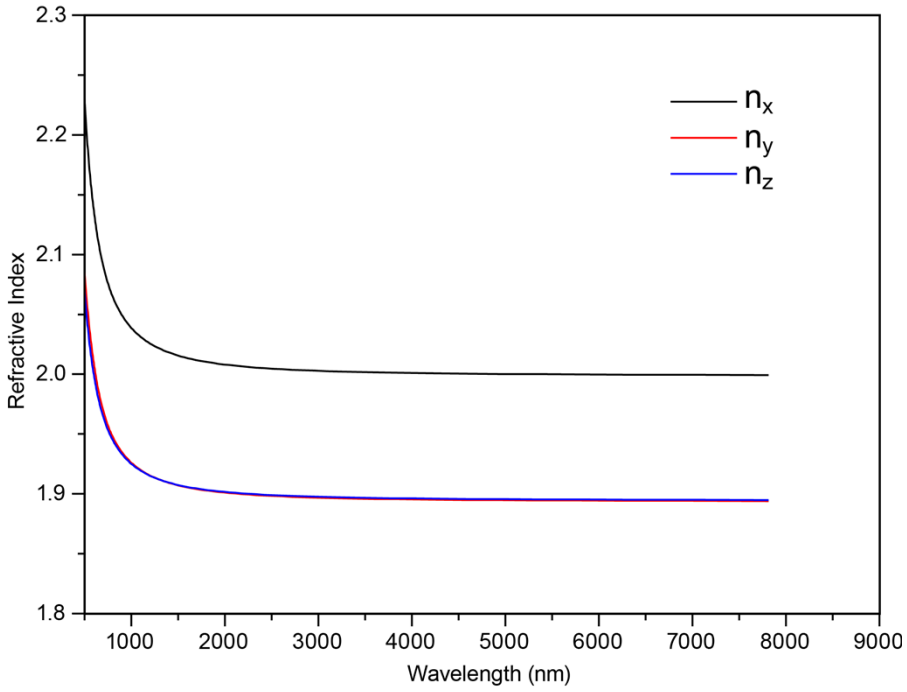

Figure S15. Calculated Refractive Indices for $Cs_2Hg_2Br_2I_4 \cdot H_2O$.

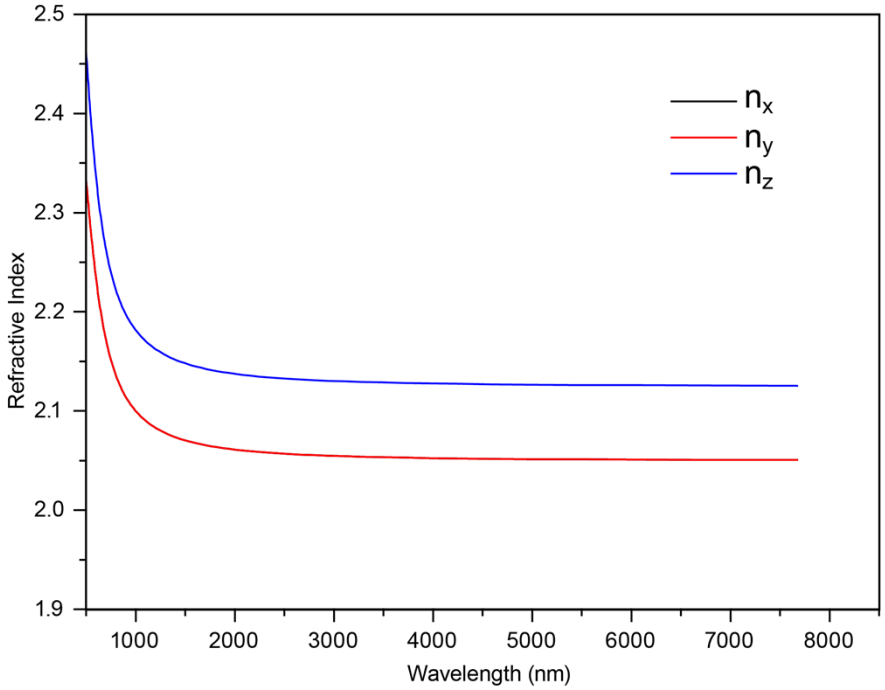

Figure S16. Calculated Refractive Indices for $Cs_2Hg_3I_8 \cdot H_2O$. In the whole wavelength range, the refractive indices n_x are the same as n_y.